14 Aug 2008, 2:30 pm - 2:40 pm

Review of Lunar Regolith Properties for Design of Low Power Lunar Excavators

Leslie S. Gertsch
Missouri University of Science and Technology, gertschl@mst.edu

Jamal Rostami
Pennsylvania State University, State College, Pennsylvania

Robert Gustafson
Orbitec, Madison, Wisconsin


6th International Conference on
Case Histories in Geotechnical Engineering, Arlington, VA, August 11-16, 2008

REVIEW OF LUNAR REGOLITH PROPERTIES FOR DESIGN OF LOW POWER LUNAR EXCAVATORS

Leslie Gertsch
Missouri University of Science and Technology
Rolla, Missouri-US 65409-0660

Jamal Rostami
Pennsylvania State University
State College, Pennsylvania-US

Robert Gustafson
Orbitec
Madison, Wisconsin-US

ABSTRACT

Lunar regolith is the product of the intermittent comminution of rocks over extremely long durations, and as such is very different from familiar terrestrial soils. A limited amount of information on lunar regolith was collected by the Apollo space program for a few locations. Additional data is required to design effective excavators to prepare outpost sites and to mine the feedstock for production of the material required for a self-sustaining crewed base on the moon. On-site manufacturing would reduce significantly the mass of material that must be launched from Earth. This paper discusses what is known and what is yet unknown about the characteristics and anticipated behavior of lunar regolith as they pertain to efficient excavation operations on the moon. It also discusses the results of tests performed on lunar simulant in dry and frozen conditions and the effects of moisture content as well as temperature on the strength of the frozen material. The results of indentation tests will be presented along with discussion of the cutting forces required for mechanical excavation of the frozen regolith. Implications of material behavior on the design of the cutterhead of excavation systems will also be reviewed.

INTRODUCTION

Permanent human presence on the moon requires a self-sustained lunar base, which in turn requires a constant supply of raw material from the lunar surface. The mass of mining/ excavation machines to meet these needs will be exceeded many times over by the mass of the material that will not have to be launched in the constant-resupply-from Earth scenario. In addition, lunar construction activities need equipment that can cope with various materials from soft surface regolith to well-consolidated regolith at greater depth, and potentially to ice-regolith mixtures. Excavation of such distinctly variable material in the Moon's hostile environment requires innovatively robust excavation systems. This paper is concerned with extracting the necessary information for designing such systems.

Lunar Regolith

Lunar regolith is produced by the continuing impact of meteorites and micrometeorites on the material that comprises the Moon. Anorthositic in the highlands and basaltic in the maria, lunar bedrock corresponds to the igneous rocks with which we are familiar on Earth, but the regolith is very different from the soil we deal with in engineering and agriculture. It contains neither biologic components nor, with a possible exception discussed below, moisture. Its grains have not been blown by wind or eroded by rain, yet they are affected by a type of weathering – space weathering – that has nothing to do with wind or rain. This is the material we must learn to handle with some efficiency if we are to make the human return to space a permanent one.

Lunar regolith can be considered to be a product of dynamic, or shock, metamorphism. The original crystalline rocks have been subjected to comminution, agglutination, vaporization and deposition from impact melting, and particle spallation and implantation by the solar wind. These processes lead to space weathering, which has implications for the formation of potential regolith ores, but that is beyond the scope of this paper.

The Clementine and Lunar Prospector missions to the Moon recorded data that could be interpreted to indicate the existence of water ice in some limited areas at the north and south poles of the Moon (Nozette *et al*., 2001). The signals also can be explained as hydrogen implanted in regolith grains by the solar wind. No direct proof of lunar ice has been obtained, but similar data from the Mars Odyssey mission is widely interpreted as convincing evidence of water ice in the near-surface regolith of Mars, and has been supplemented by additional lines of evidence (Boynton *et al*, 2002 and others). The composition of the potential lunar ice may be similar to the average cometary composition of 79% H_2O, 7% CH_4, 7% NH_3, and 7% H_2CO (Duke, 1989), but this is uncertain.

Excavatability of Lunar Regolith

Much of the engineering we do with soil and rock on the Earth is based on empirical observations and traditions built on long

experience. This has served well enough, if not perfectly. Though we have only the barest beginning of a body of experience with lunar regolith, much information has been collected about it. Some is of use for the design of excavation systems. Table 1 summarizes the major physical property measurements and estimates for lunar regolith. In addition to the information listed in this table, cone-penetrometer measurements from Apollos 14, 15, and 16 show that resistance to penetration increases as a function of depth.

The physical properties of frozen soil are sensitive to several factors, including water content, temperature, and particle size distribution. We can infer some properties of ice and regolith mixtures on the Moon from terrestrial experience with frozen soils and permafrost. Much of the terrestrial data are at higher temperatures and water ice content than we expect on the Moon, so they can not be used directly. However, some can be interpolated to the temperatures and moisture levels of interest.

The variation of the uniaxial compressive strength of frozen soils as a function of their water content is basically the same for all types of frozen soil (Fig. 1). The compressive strength of dry soil is point O. The compressive strength of frozen soil increases rapidly with increasing water content until the soil becomes saturated (point A). The saturated frozen soil mixture has the highest compressive strength. As the water content of the soil increases beyond the saturation level, the strength of the mixture decreases (curve segment AB). As the water content is further increased, the compressive strength continues to decrease below the compressive strength of pure ice (curve segment BC). At higher water content, the compressive strength remains fairly constant (curve segment CD). As the water content of the soil is further increased, the compressive strength of the frozen soil approaches the value for pure ice (curve segment DE).

Table 2 shows estimates of the *in situ* porosity of the lunar regolith; the average from 0-60 cm depth is 43%. Given the average density of individual lunar regolith grains of 3.1 g/cm^3, and the average ice density of 0.92 g/cm^3, the saturated lunar regolith would contain 18.9% water ice by mass.

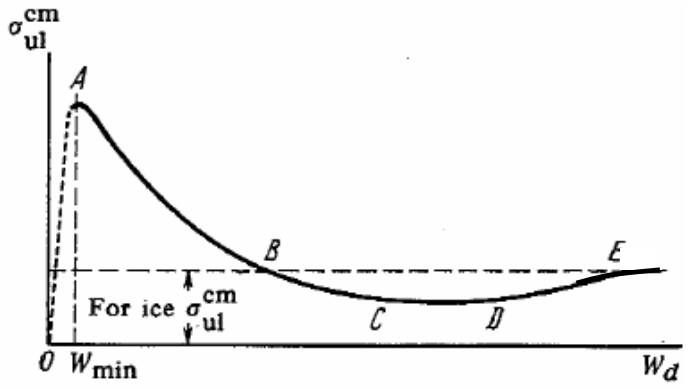

Fig. 1. Uniaxial compressive strength of frozen soils as a function of water content (after Tsytovich, 1975).

Table 2. Best estimates of lunar regolith *in situ* porosity (Heiken *et al*., 1991).

Depth Range (cm)	Average Porosity, n (%)	Average Void Ratio, e
0 - 15	52 ± 2	1.07 ± 0.07
0 - 30	49 ± 2	0.96 ± 0.07
30 - 60	44 ± 2	0.78 ± 0.07
0 - 60	46 ± 2	0.87 ± 0.07

If the hydrogen concentrations measured by Lunar Prospector are in the form of water, the average ice content of the regolith in the permanently-shadowed craters near the lunar poles is estimated to be 1.5 ± 0.8% by mass. It is likely that the ice-rich regolith is covered by a layer of relatively dry regolith. However, the resolution of these data is tens of kilometers per pixel. Therefore, it is impossible to characterize the local variations of ice within the regolith. Recent analysis of the Lunar Prospector data indicates that local ice concentrations probably exist in excess of 10% by mass.

Fig. 2 compares the compressive strength of several terrestrial frozen soils with different particle size distributions. In general, frozen soils with larger particle sizes (*e.g.*, sand) are stronger than those with smaller particle sizes (*e.g.*, clay). Lunar regolith average particle size is between sand and clay.

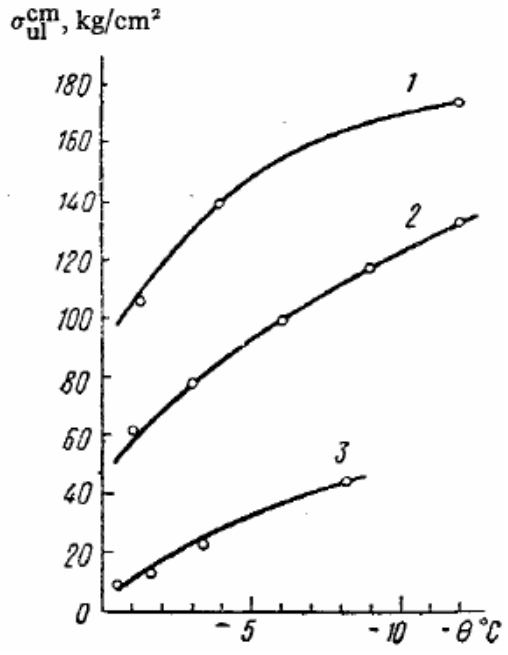

Fig. 2. Ultimate compressive strength of frozen terrestrial soils as a function of temperature for (1) sand, (2) sandy loam, and (3) clay (Tsytovich, 1975).

Table 1. Summary of the geotechnical measurements and estimates for lunar regolith.

Mission	Basis	Density (g/cm^3)	Cohesion (kN/m^2)	Friction Angle (deg)	Porosity	Void Ratio	Reference
Orbiter	Boulder track analysis		0.35	33			Nordmeyer (1967)
Surveyor I	Strain gage and TV data		0.15-15	55			Jaffe (1967)
Surveyor I		1.5	0.13-0.4	30-40			Christensen et al. (1967)
Luna 13		0.8					Cherkasov et al. (1968)
Surveyor III	Soil mechanics surface samples			>35			Scott and Roberson (1968)
Surveyor VI	Vernier engine firing		>0.07	35			Christensen et al. (1968a)
Surveyor VI	Altitude control jets		0.5-1.7				Christensen et al. (1968a)
Surveyor III and VII							Scott and Roberson (1967, 1968) and Scott (1968)
Surveyor III and VII	Soil mechanics surface samples		0.35-0.70	35-37			Scott and Roberson (1969)
Lunar Orbiter	Boulder track analysis		0.1	10-30			Moore (1970)
Lunar Orbiter	Boulder track analysis		0.5 (assumed)	21-55 (mean 39)			Hovlan and Mitchell (1971)
Apollo 11	Footprints, LM landing data, crater slope stability		Consistent with Surveyor soil model				Costes et al. (1969)
Apollo 11	Penetrometer tests in LRL on bulk soil sample		0.3-1.4	35-45			Costes et al. (1970)
Apollo 11	Penetration of core tubes, flagpole, SWC shaft		0.8-2.1	37-45			Costes et al. (1971)
Apollo 11		1.54-1.75					Costes and Mitchell (1970)
Apollo 11		0.74->1.75					Scott et al. (1971)
Apollo 11		1.81-1.92					Costes et al (1971)
Apollo 11		1.6-2.0					Scott et al. (1971)
Apollo 12	Footprints, LM landing data, crater slope stability		Consistent with Surveyor soil model				Scott et al. (1970)
Apollo 12	Penetration of core tubes, flagpole, SWC shaft		0.6-0.8	38-44			Costes et al. (1971)
Apollo 12		1.80-1.84					Costes et al. (1971)
Apollo 12		1.55-1.90					Houston and Namiq (1971)
Apollo 12		1.7-1.9					Carrier et al. (1971)
Luna 16		1.2					Vinogradov (1971)
Lunokhod I		1.5-1.7					Leonovish et al. (1971)
Apollo 14	Soil mechanics trench		<0.03-0.3	35-45			Mitchell et al. (1971b)
Apollo 14	Apollo simple penetrometer		Soil shear strength >/= Surveyor data				Mitchell et al. (1971b)
Apollo 14	MET tracks			37-47			Mitchell et al. (1971b)
Apollo 14		1.45-1.6					Carrier et al. (1972)
Apollo 15		1.35-2.15					Mitchell et al. (1972)
Apollo 15	Measured at Station 8	1.92-2.01 (typical 1.97)		47.5-51.5 (typical 49.5)	35-38 (typical 36.5)	0.54-0.61 (best 0.58)	Mitchell et al. (1972)
Apollo 11, 12, 14, 15		1.76	0.55	43	43.3		Houston et al. (1972)

The mechanical behavior of ice molecules is characterized by very weak hydrogen bonds. However, there is a sharp decrease in the mobility of the hydrogen bonds as the temperature decreases. This reduced mobility significantly strengthens the ice structure. Figure 3 shows how the shear strength of ice and frozen soils increases as the temperature is lowered. Ice strength increases 5 to 10 times when temperature decreases from 273 K to 150 K. The strength of the ice below 150 K remains approximately constant.

The ice that may be present in the lunar cold trap regions could be amorphous or crystalline. The temperature within the permanently-shadowed lunar polar regions may be as low as 30-50 K. At these temperatures, water vapor generally forms low-density amorphous ice. However, this is a relatively unstable phase, and if the temperature rises above 120 K, it rapidly transforms into crystalline ice. Heat is released during this transition since the crystalline form of ice is a lower energy state. The released heat would cause the surrounding ice also to change and to release additional heat. Therefore, even if the lunar ice is naturally amorphous, it will likely crystallize during excavation.

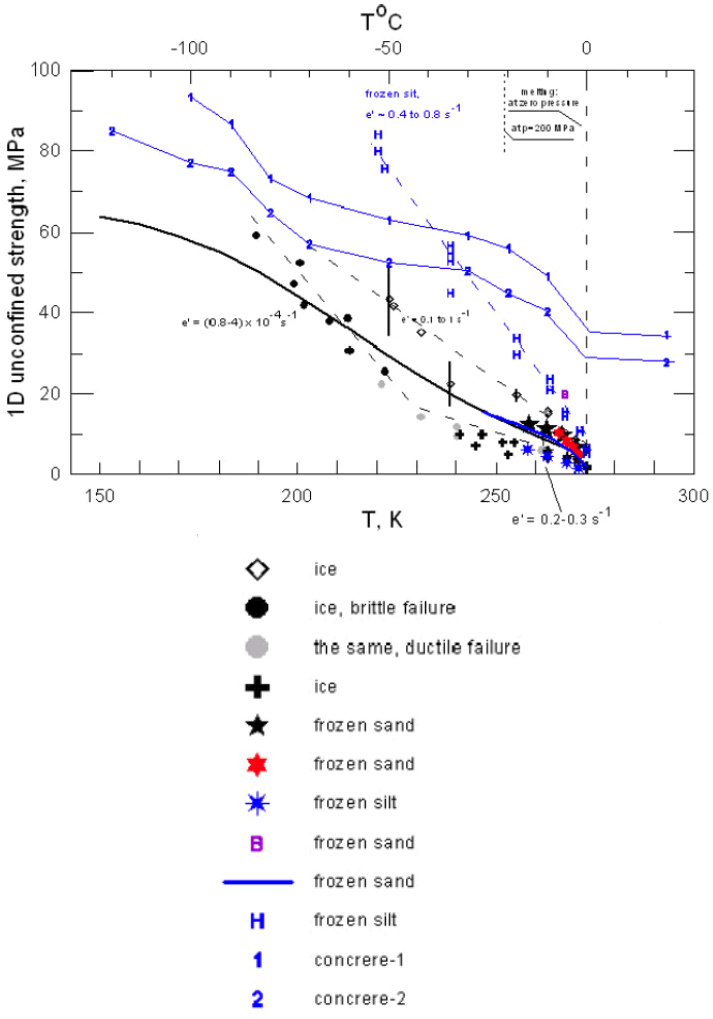

Fig. 3. Unconfined shear strength of ice and frozen soils as a function of temperature (Ivanov, 2001).

However, the lunar ice may not even be amorphous initially. Amorphous ice was expected on Pluto's moon Charon, since the temperature never exceeds 80 K and is more typically in the 35-50 K range. Ultraviolet rays from the Sun and cosmic radiation should slowly disrupt the organized pattern of hydrogen bonds that accounts for the structure of crystalline ice, producing the amorphous form near the surface. However, infrared spectra of Charon show that the ice there is in fact predominantly crystalline rather than amorphous (Brown and Calvin, 2000; Young, 2000). The reason for this is not entirely clear. Meteorite bombardment (*i.e.*, vibratory disturbance) is one possibility, or some process that has not yet been considered.

Given the uncertainty about the form of the lunar ice and the difficulty in creating uniform mixtures of lunar regolith simulant and amorphous ice, the samples produced for testing used crystalline ice. Liquid water was mixed with JSC-1 lunar regolith simulant, compacted, and then immersed in a liquid nitrogen bath (~77 K). This process produced a mixture of crystalline ice and lunar regolith simulant. An argument can be made that force indentation tests with crystalline ice-regolith simulant mixtures is more useful from a mining perspective. Even if amorphous ice exists on the moon, it is very unstable and it will likely transition to the crystalline form during excavation due to the increased temperature and pressure beneath an excavator tool.

Lunar Regolith Simulant

The amount of lunar regolith returned from the Moon by both Russian and American missions is too valuable for other studies to be available in the quantities needed for excavator system design. Accordingly, several types of artificial lunar regolith simulants have been created. The work reported here used a type referred to as JSC-1.

Mechanical Excavation

The production of geologic materials consists of several unit operations: fragmentation (breaking it away from its surrounding material), loading, hauling, comminution, and separation. Mechanical excavators rely on mechanical rather than explosive energy for fragmentation, and can combine many sequential unit operations in one machine. The quality of the initial fragmentation is crucial to all subsequent stages of processing, and thus to the success of mining and excavation activities.

Mechanical excavators have been used in both underground and surface applications for over two hundred years (Stack, 1982). The earliest coal cutter was invented in 1761, and the first soft-ground tunnel-boring machine (TBM) was built in 1816; the modern hard-rock TBM was invented in the early 1950's. Mechanical methods have long been a staple of coal mining, and account for almost all coal produced underground in the US. Modern application of mechanical excavators to large surface mines began in the early 1980's in open pit coal mines (National Gypsum, 1995), where drum mining machines were adapted from underground coal mining machines and from road-asphalt milling machines. Presently, continuous surface miners can operate economically in compacted, but otherwise unconsoli-

dated material such as sand, gravel, and clay, and in rocks with strength below about 80 MPa (*e.g.* coals, bauxite, soft sandstone, phosphate, gypsum, and marl). They are well suited for selective mining of layers or seams that are too competent or too thick to be removed directly with a bowl scraper.

Mechanical mining machines will be most effective in soft to medium-strength extra-terrestrial materials, such as lunar regolith and the friable classes of asteroids. Since mechanical mining is a mature and well-understood terrestrial method, they are readily adaptable for a wide variety of space applications, from very small exploration samplers to very large machines that provide material for self-sustaining bases in space. They are also suitable for automation and robotics, reducing the need for human intervention and operation. In addition, the product size from these machines can be directly fed to all types of transportation systems and finally to most processing plants without the need for additional comminution. Although regolith is already well-comminuted, the cementing action of ice will cause it to react more like rock than like soil to the indentation of cutting tools.

Some direct transfer of terrestrial excavator technology to the Moon is feasible without a significant change in design philosophy. Current design practice focuses on the excavatability of a specific target material, resulting in site- or material-specific machines that cannot operate efficiently in other materials. Lunar regolith miners are expected to operate in materials whose properties and spatial variability are not well-defined. In addition, the demands of the lunar environment will exceed those of the toughest mining environments on Earth, requiring additional robustness to forestall unexpected problems and to facilitate maintenance and repair.

Excavator Design

Mechanical excavators consist of four main subsystems: the power plant or drive system, the cutterhead, the materials handling and loading systems, and the carriage. Fragmentation is accomplished by the cutterhead: a rotating device, mounted with cutting tools, that applies force to the target material in the necessary magnitude and configuration to cause it to break away from the surrounding material. The cutting tools can be of many designs, from picks to drag bits to disc cutters. The cutter type and layout on the cutterhead are selected to match the properties of the material being excavated. The cutterhead continually moves tools through and across the material in a rotating motion.

The transport system must keep up with the cutterhead by removing the excavated material as fast as it is created, to prevent unnecessary energy expenditure for regrinding and rehandling. The carriage must maintain enough stiffness, mass, and power to operate the cutterhead and the transport system, and provide sufficient thrust and torque to fragment the material effectively. Insufficient stiffness and torque result in a machine that is too compliant, which creates damaging machine vibrations and lowers production rate. The power plant, or drive unit, provides power for all systems. A beneficiation module can be integrated with the mining system to avoid transportation of high volumes of material to a central processing unit. For regolith mining, this entails separating waste particles from ore particles according to whatever properties are required. For simple excavation, as for site preparation, beneficiation may be limited to removal of over-size rocks.

Cutterhead Design. The most important subsystem in the mechanical excavator is the cutterhead. The entire machine is designed around the geometry of the array of cutters, the shape and size of the cutters, and the resulting forces on the cutters. The essential design element for the cutterhead (and hence the entire machine) is the forces that develop on each individual cutter as it fragments the material. The interaction of spacing, penetration, and material strength is the crucial element that controls design of the entire excavator. In weak rock, cutting forces are low; consequently, cutter penetration into the rock and the spacing between the cutters can be large. In strong rock, cutting forces are high; consequently, cutter penetration and spacing must be small. Therefore, fewer cutters are needed on the machine and more material is excavated for a given amount of energy if the rock is weak. The converse is true for strong rock; less material is excavated for the same amount of energy.

The forces on a cutter are due to a combination of the target material's resistance to penetration and its propensity to form chips when penetrated. As each individual cutter penetrates the material, two types of failure occur: (1) material directly under the cutter is finely crushed, and (2) chips or large fragments form in front and to the side of the cutter's path. The larger the chips, the more efficient the fragmentation process, because the energy consumed is inversely proportional to the new surface area created. More efficient cutterheads produce more chips than small particles (fines). Additionally, cutter forces determine the power needed to achieve certain production rate.

For design purposes, cutter forces are estimated by two methods: direct measurement, and the use of empirical formulas. The most reliable prediction of machine performance results from full-scale cutting tests, by directly measuring the cutter forces required to achieve a pre-set penetration of the material given a pre-set spacing between cuts. This is feasible when large (>0.3 m^3) samples of material are available. Cutting is performed under a range of spacings and penetrations to identify the optimum combination with the lowest specific energy requirements. This method can pinpoint production rate to within ± 10% in terrestrial practice.

Alternatively, empirical formulas can also be used to predict cutting forces. They use uniaxial compressive strength (UCS) of the material as the most common indicator of rock strength and cutability. Specific penetration (SP), a characteristic measured by load-indentation (punch) tests, can also be used for cutting force prediction. Other properties such as tensile strength, shear strength, modulus of elasticity, modulus of rupture, degree of pre-existing fracturing, sonic wave velocities, Poisson's ratio, and density also can be combined to estimate cutting forces.

Another important issue is cutter wear, which is related to cutter and material strength and brittleness, and material abrasivity. In

rock or soil excavation, abrasivity is ordinarily measured as the percent of quartz in the material, but can also be expressed by various indices such as Cerchar abrasivity, Shore scleroscope hardness, *etc*.

Cutterhead design methodology begins by selecting a proper cutter / bit followed by selection of an optimum ratio of cutter spacing to penetration for a specific material to be cut. The cutterhead power must be sufficient to provide the necessary force for each cutter in contact with the material to achieve the critical penetration to cause chipping. Selection of reasonable cutterhead rotational speed and other system parameters then permits estimation of the volume of material excavated The machine carriage must be able to support all the subsystems in the operating environment in a robust yet flexible manner.

Cutter Forces. Cutterhead design and modeling starts with estimating cutting force on an individual cutter, predicted from force penetration curves. The two main components of force are the normal and drag forces, which are radial and tangential forces relative to the axis of rotation, respectively. The tangential force resists rotation of the cutterhead, and the parallel force resists its forward motion.

Shearing Forces. The forces on the cutters in contact with the material are summed in the direction of travel to calculate machine shearing or traction force. Depending on the depth of the slice to be cut, only a few cutters will be in contact with the regolith at any given time. The total traction force is the sum of the thrust components on those cutters.

Torque. The torque on the cutterhead is a function of the cutterhead diameter and the number of cutters, as well as the cutter tangential (drag) force. Total cutterhead torque is the sum of the torques from the cutters in the contact area. It is useful to note that, although the traction force (parallel force in the direction of machine movement) acting on a cutter is higher than the tangential force, the energy required for excavation is determined primarily by torque. This is due to the fact that the displacement of each cutter in the tangential direction is many times greater than its displacement in the direction of advance.

Rotation Rate - Cutterhead Power - Production Rate. Cutterhead power is the cutterhead torques multiplied by the cutter velocities at the selected rotation rate. Once the penetration is determined by the available traction forces and bit load capacity, cutterhead rotation rate can be selected to maximize production rate. The production rate is a function of the depth of slice to be cut and the speed of forward motion, which is determined by the depth of penetration and the rotational speed of the cutterhead.

EXCAVATABILITY TESTING

A characterization program of the physical and mechanical properties of soils and rocks related to their excavatability was undertaken as the starting point for excavator design. To gain a better understanding of the potential range of physical properties that may be encountered in excavation operations, various mixtures of ice and lunar regolith simulant were created, the strength of the samples were measured, and their load-indentation behavior was observed.

The standard technique presses a hemispherical indenter into the material at a rate approximating the strain rate of an active cutting tool, and to record the force required versus displacement (Dollinger, 1978; Dollinger *et al*., 1998). The parameters of interest calculated from this test are specific penetration (SP) and specific energy (SE). Specific penetration (Gertsch, 2000) is a measure of the force necessary to achieve the critical penetration required to form chips. It is obtained from the slope of the initial ramp of the sawtooth force curve that results from indentation (see Fig. 6). The amount of energy required to excavate a unit volume of material is the specific energy (SE).

Sample Preparation

After the saturation point of the JSC-1 lunar regolith simulant had been determined experimentally, saturated simulant mixtures were formed by adding simulant to a pre-measured amount of water in a transparent container. The water and simulant were thoroughly stirred as more simulant was added. The stirring also helped to release small gas bubbles that appeared to be trapped in the pores of the simulant. Additional simulant was added to the mixture until the upper level of the simulant nearly coincided with the water level, after which the simulant mixture was allowed to settle for several hours. Any water present above the simulant was then carefully removed. The remaining mixture was considered fully saturated. The mixture was weighed and then baked at 250°C for three days to remove all water. Two different techniques were then used to determine the amount of water in the samples, which turned out to be similar to the estimated porosity, converted to mass fraction (19.6%).

By mechanically mixing various amounts of water with dry JSC-1 lunar regolith simulant, samples with water concentrations ranging from less than 1% to full saturation were produced. Multiple samples taken from single batchesverified that they were homogenous. Then, portions of each mixture were compressed into stainless steel test rings with closed bottoms.

Vibratory compaction turned out to be more effective than static mechanical compression for inducing the appropriate density in the samples. During Phase 1, all samples were compacted by applying a static stress of 56 MPa, which produced 77% relative density for the dry samples, and 56% relative density for the saturated samples. During Phase 2, fully dry and fully saturated samples were successfully compacted using vertical vibrations with peak accelerations of 2.9 gravities, producing relative densities up to 100% (dry) and 91% (saturated). This proved to be ineffective, however, for compacting JSC-1 simulant mixed with intermediate amounts of water. An attempt with a water content of 7 wt% produced a relative density of only about 28%.

Sample compaction was followed by sealing and immersion in a liquid nitrogen bath to cool the mixture to approximately -196ºC (77 K). A Type K thermocouple was located inside each sample to verify its internal temperature.

Load-Indentation Testing

The load-indentation testing (Fig. 4) was performed under ambient laboratory conditions, although the elapsed time between removal from the liquid nitrogen dewar and indentation was kept to less than two minutes. Testing consisted of pushing a 19-mm diameter hemispherical steel indenter perpendicularly into the center of the top surface of the prepared sample, at a displacement rate of 1.24 mm/sec. After reaching a maximum penetration of 9 mm, or achieving multiple chipping episodes, the indenter was withdrawn and the sample was photographed (Fig. 5). It was then sealed into a water-tight bag and thawed in preparation for dissection. This entailed careful removal of first the surface chips, then the finer fragments (Fig. 6). The fines included a "button" of highly compressed material that formed directly beneath the indenter. Sample dissection provides information for determining the total failure volume, as well as the relative proportions of small and large fragments, which conveys information about the efficiency of the fragmentation.

Fig. 4. A sample ready for indentation.

Fig. 5. Close view of a sample immediately after indentation, showing some of the chips and the fines produced.

Fig. 6. Some samples were dissected following indentation, to determine the relative proportions of fines and chips, and the total size of the failed zone.

Results

Failure in the dry simulant samples is semi-ductile, with material often doming around the sides of the indentation. This indicates that the material can be excavated with a backhoe or similar low-force excavator and may not require a cutterhead. This conclusion is supported by the very low failure loads and relatively deep first-failure penetrations of the dry samples (Fig. 6). However, they were compacted statically; vibratory compaction might make this behavior more rock-like by increasing the grain interlocking without concomitant damage.

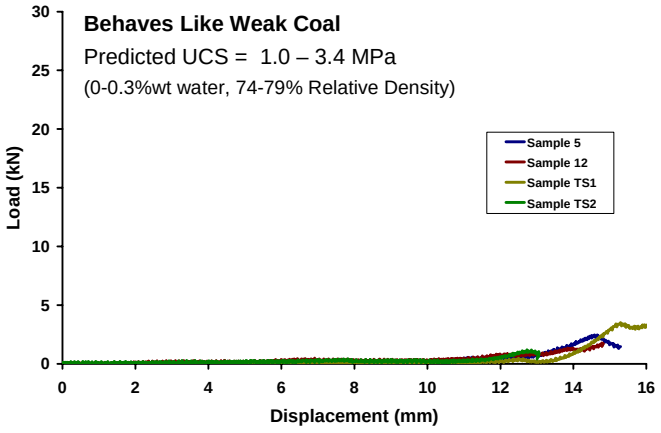

Fig. 7. Force-indentation curves for <0.3% moisture, in samples compacted statically.

Failures in the mixtures containing water ice are more characteristic of brittle rock (Fig. 8); they are typified by large flat chips that form around the periphery of the indenter, and a report (audible crack) upon failure of each chip. Chips would occasionally hop out of the test ring. Many chip formation events coincide with load spikes followed by sharp unloads, leading to gradual reloading (Fig. 9-12). The reports appear to occur during the load drop-offs. This cyclic sawtooth failure behavior, and the concurrent formation of a consolidated crushed zone below the indenter, are also characteristic of brittle rock failure under indentation. Also similar to rock, the frozen saturated simulant is strong in compression, while weak in tension.

Examination of the individual load-indentation test plots reveals additional features of indenter behavior that bear on excavator cutterhead design and performance. At zero to low water contents, significant penetration occurs before the indenter experiences any significant resistive force. As water content increases, the first-failure force climbs and, as water content continues to increase, the material begins resisting earlier in the penetration and continues to relatively high failure load. Another way to describe this behavior is to say that the brittleness increases with water content. At 77 K ice behaves more like a strong brittle material than a collection of dry regolith particles, which behave like a ductile material in the aggregate. Material with the highest water contents – approximately saturated – loads rapidly, fails at shallow penetration, then rapidly reloads and fails again several times in succession. These materials don't "give up" as readily as drier regolith simulant mixtures; they continue to resist as indentation increases.

The SP results (Fig. 13) reflect regolith behavior only during actual loading to the first failure, whereas the excavated volumes shown in Fig. 14 reflect behavior over entire tests. Thus they represent slightly different timescales. Specific energy, in Fig. 15, combines two full-test measures: total energy expended and total volume excavated. Table 3 summarizes the qualitative results of the tests.

Fig. 8. The brittle, energetic failure pattern typical of saturated samples.

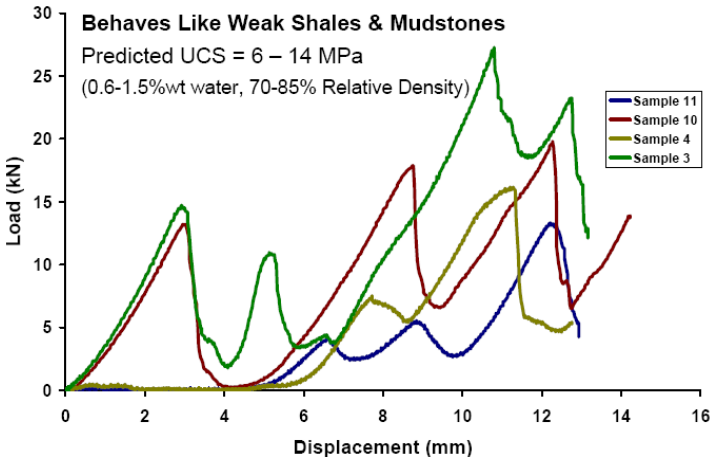

Fig. 9. Force-indentation curves for ~1.1% moisture, in samples compacted statically.

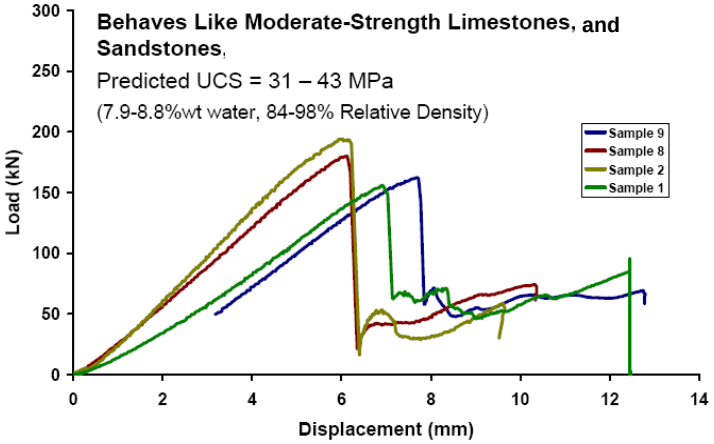

Fig. 10. Force-indentation curves for ~8.1% moisture, in samples compacted statically. (Note the Y-axis scale is one order of magnitude greater than in Fig. 7 and 9.)

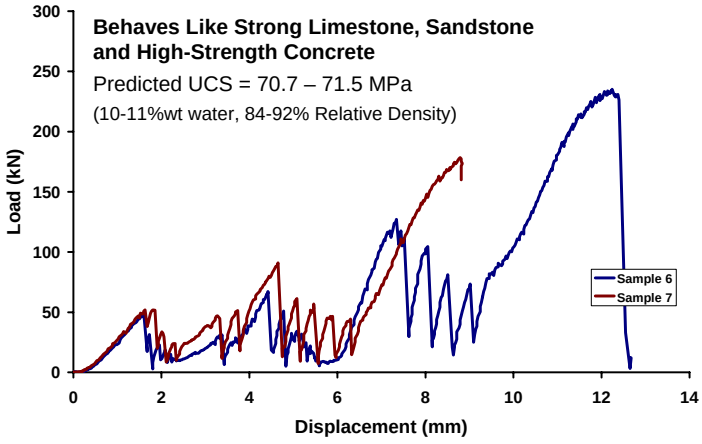

Fig. 11. Force-indentation curves for ~10.5% moisture, in samples compacted statically.

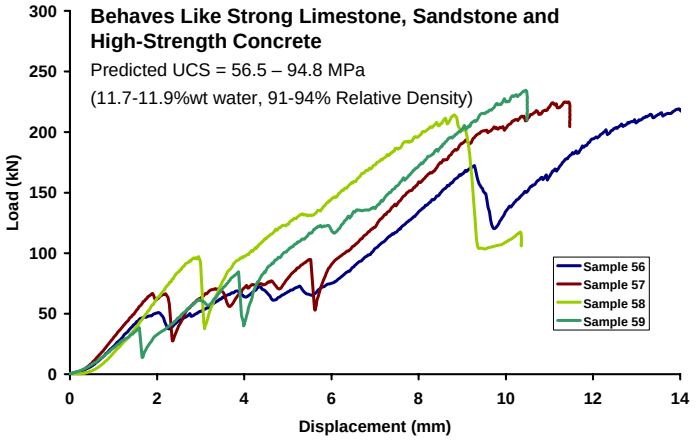

Fig. 12. Force-indentation curves for ~11.8% moisture, in samples compacted by vertical vibration.

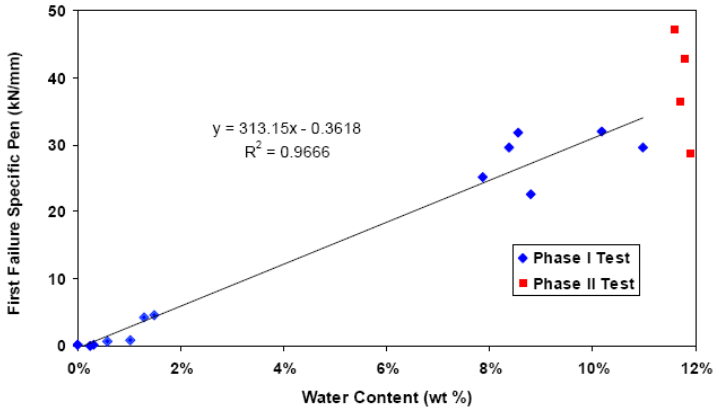

Fig. 13. First-failure specific penetration versus % water ice content.

The data in Fig. 13 may show an abrupt change of behavior at about 1.5% ice concentration. The small number of data points makes this a tentative conclusion at best, and Phase II data indicate wide variability in the results, but if this reflects a true failure regime change, it would have large consequences for excavator performance. The reason is that the widely accepted model of intergranular ice in the lunar polar cold traps predicts 1.5 ± 0.8% average concentration. Since the apparent threshold is squarely within this range, excavators working in those deposits may have to operate in two different regolith failure regimes, with different attendant cutterhead requirements.

Dry samples produce large failed zones. Even a very small amount of ice in the mix significantly and nonlinearly decreases the excavated volume (Fig. 14). Higher moisture content thus would lead directly to lower production rates. When the excavated volume goes down and cutting force does not change significantly, the cut spacing required for minimum energy expenditure is reduced as well; if it were not, the material would not fragment between cuts, but would remain as difficult-to-remove ridges that increase abrasion and wear on the cutterhead. When such ridges do finally break apart, they form large chunks that are difficult for the material transfer system to handle.

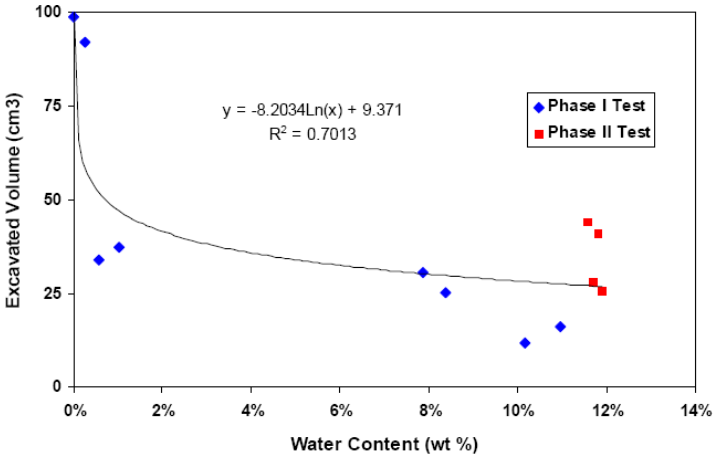

Fig. 14. Excavated volume versus water ice content.

The SE, like the SP, increases significantly with ice content (Fig. 15). Any excavator will require unprecedented flexibility wherever the ice content varies more than a percent or two from the target. This is an especially crucial finding for a location with low power supplied and little or no repair capabilities.

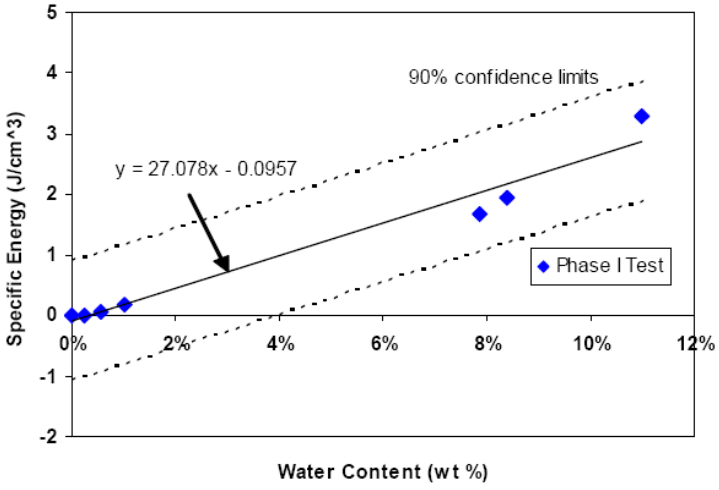

Fig. 15. Specific energy of fragmentation versus water ice content.

Table 3. Effect of water content load-indentation behavior.

Ice Content	Penetration at First Failure	Excavated Volume	Load at First Failure
None	Deep	Large	Low
Low	Deep	Large	Low-Moderate
Moderate	Deep	Moderate-Large	Moderate
High	Deep	Moderate	High
Saturated	Shallow	Small	Very High

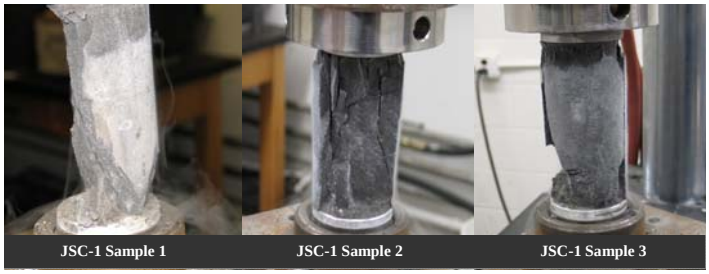

Fig. 16. Examples of frozen saturated JSC-1 lunar regolith simulant samples after direct UCS measurement.

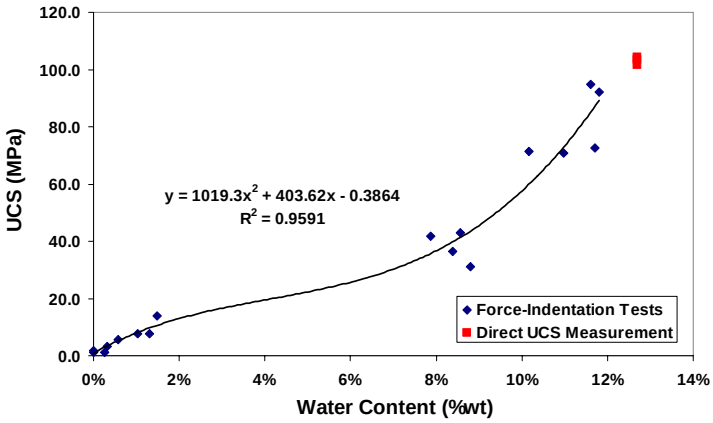

Fig. 17. Variation of UCS as a function of water content in compacted JSC-1 lunar regolith simulant at ~77 K.

Cylindrical samples of the saturated lunar regolith simulant were also prepared for direct measurement of the UCS. The sample was prepared in a split cylindrical mode following ASTM D4253 and tested according to ASTM D4543. Figure 16 shows some of the samples after failure. The testing determined that the UCS of saturated JSC-1 lunar regolith simulant is 102-104 MPa, which aligns well with the UCS predicted from the SP values (Fig. 17).

LINEAR CUTTING TESTS

The basis for calculating the operating parameters of an excavator – thrust force into the regolith, rotational torque, and total power – is the cutting force needed to achieve a given penetration of the cutters into the target material. This basic measurement, obtained from the load-indentation tests described above, is then confirmed by full-scale linear cutting tests using a specific bit in a large sample of the target material.

These tests were performed for this study at the Kennametal Rock Cutting Laboratory in Latrobe, PA. Two different conical bits were evaluated in a 48 ft^3 block of Salem Limestone (Fig. 18). This widely available type of dimension stone was selected for its similarity to the 8% water ice-regolith simulant mixtures in terms of both SP and UCS. Cutter spacings of 25, 50, and 75 mm, combined with penetrations of 2.5, 5.0, and 7.5 mm, were tested. In addition, visual observations of the cutting surface were made and representative samples of the failed material were collected (Fig. 19-20). The numerical results are currently being analyzed.

The optimum spacing between cutters can be estimated from the results of linear cutting tests. The optimum spacing depends on the cutting forces and the specific energy of fragmentation. SE gives the maximum cut spacing for which the allowable bit forces (determined by the power, thrust, and torque limits of the excavator) can achieve a certain penetration. The optimum ratio of spacing to penetration (S/P ratio) is that for which the critical penetration necessary to achieve full excavation between cutter paths is just reached. These tests indicate that the optimum S/P ratio for this bit in this material is approximately 5, meaning that if the maximum anticipated penetration is 7.5-10 mm, the corresponding spacing should be 37-50 mm for optimum cutting efficiency.

Fig. 18. Linear cutting test of a conical bit in Salem Limestone.

Fig. 19. Typical fragmentation when critical penetration is reached. S/P ratio is 3.3.

Fig. 20. Typical fragmentation when critical penetration has not been reached. S/P ratio is 10.

These results will be further evaluated by a series of rotational cutting tests. Each test series more fully approximates the actual *in situ* cutting behavior than the previous series, and the design of each is informed by the results of its predecessors.

PRACTICAL IMPLICATIONS

Cutterhead Design

Designing a cutterhead is an iterative process, where an initial cutterhead lacing pattern is selected and the related operating parameters are calculated. These parameters are then compared to the desired machine specifications, to see if a given machine can support such cutting geometries. If the required machine parameters exceed available capacities, the lacing is modified and new operating parameters are calculated. The process continues until the design cutterhead exhibits reasonably low energy consumption while maintaining a sufficient number of cutters in contact with the cutting surface to ensure that force and torque variations are minimized. The iterative process is necessary to reach a balance between the number of cutters and the resulting force and torque variations. Increasing the number of cutters increases the total cutterhead thrust and torque requirements, thereby increasing energy consumption. Reducing the number of cutters can lead to incomplete cutting between the lines and higher vibrations, which negatively impact machine operating life and performance.

A simple computerized excavation model was developed to predict cutterhead performance. The input parameters include cutter spacing and penetration, drum rotation rate, drum diameter, drum length, and material strength. These parameters were systematically varied and the resulting changes in machine thrust, torque, power, and production rate are calculated. The model is supplemented by observation of cutterhead behavior. It allows the user to perform design optimization without having to test all potential combinations at full scale, by calibrating the model with selected cutting tests.

Cutter Spacing. Selecting spacing between cutter tracks involves some judgment based on experience. The starting point is current terrestrial practice. Most mechanical excavators have cutter spacings of 50 to 100 mm. This range is appropriate for materials of moderate strength, defined as less than 100 MPa uniaxial compressive strength (UCS). This nearly covers the range of anticipated compressive strength of the frozen regolith. Cutter spacing is also controlled by the size of the bit and the mass of the machine. As noted before, the optimum S/P ratio is used as a guide for selecting the spacing, which determines the necessary penetration, which in turn requires a certain bit loading capacity. Excavator thrust, torque, and power are back-calculated from the number of bits in contact at any given time. Most common terrestrial excavators, massing 50-100 tons, can provide over 1-2 tons of load on each bit. This is usually sufficient to reach the critical penetration depth for efficient fragmentation. Thus regarding cut spacing the following conclusions can be reached:

1. All the measured UCS values for the frozen lunar simulant are below 104 MPa; therefore, all water ice contents can be fragmented by cutterheads laced with typical conical bits.
2. For simulant with low or no water ice content, the material should be relatively easy to excavate mechanically at relatively wide cutter spacings.
3. For simulant with high water ice content, the predicted UCS and average SP values are much higher than for the other simulants; therefore, the optimum cutter spacing is narrower.

Comparing UCS and SP for the simulant samples to a terrestrial continuum (Tables 4-5) sheds further light on the selection of an energy-efficient cutter spacing. The mineral anhydrite has a UCS of 10 MPa and a SP of 16 kN/mm. These values are close to those observed for a water ice concentration of 1.5% in JSC-1 lunar simulant. Lower concentrations, in the range of 0.5-1.5% water ice, have UCS and SP values of ~5 and 7, respectively. Anhydrite is commercially excavated by road milling machines or similar miners at cutter spacings of 50-75 mm. The 1.5% concentration appears to be a transition from soft to moderately strong material. Although the exploratory test program has few data points, it appears that compacted JSC-1 regolith simulant quickly gains strength at a relatively low water ice concentration. If the phenomenon holds true, mechanical excavation for frozen regolith may present material that varies widely in strength, since water ice concentrations on the Moon could well range from near zero to near saturation.

Analysis of Tables 4 and 5 also provides reasonable cutter spacing for lunar simulant with water ice concentrations less than about 1.5%. In this range, two strength groups are apparent, although more tests are needed to fully explore this behavior. The lowest strength group has SP values of about 1 kN/mm and UCS of about 1-2 MPa. The somewhat higher strength material has SP values of about 5kN/mm and UCS of about 7 MPa. The higher strength material is similar in this way to low-strength steam-coal and shale. These materials are excavated in

underground mines and civil excavations at cutter spacings of 50-100 mm. Narrower spacings are used when smaller machines are required for reasons other than efficient fragmentation.

The lowest-strength sample tested, with SP of about 1, is like partially consolidated soil and can likely be excavated by shovels. This type of material is not commonly dug with bits, so a relatively wide spacing of 100 mm should be sufficient.

When the moisture concentration reaches 8-10%, the mixture becomes much stronger and is now in the range of moderately strong rocks mined by mechanical excavation. The ~8% water ice material exhibits SP values of 20-28 kN/mm and UCS values of 31-43 MPa (Table 5). Terrestrial analogs of moderate strength shale, sandstone, and limestone are commonly excavated with 50 mm cutter spacing, although it can be wider if the rock contains minimal natural cement. Indentation testing of these samples showed that after the first failure the material behaves plastically and is slow to reload for the remainder of the test (Fig. 10). Although the first failure indicated relatively wide spacing, the continuing plastic behavior argues for narrower spacing. Thus a conservative, narrow spacing of 50 mm is recommended.

Table 4. Typical specific penetration (SP) and uniaxial compressive strength (UCS) values for a range of terrestrial rock types (Farmer, 1968 and Gertsch, 2000a).

Rock Type	Avg SP (kN/mm)	UCS (MPa)
Coal	3-32	5-50
Shale	6-65	9-90
Sandstone	13-110	19-170
Anhydrite	10	16
Gypsum	15	22
Limestone	26	38
Welded tuff	69	99
Limestone	89	127
Granite	112	158

Table 5. Specific penetration (SP) and predicted uniaxial compressive strength (UCS) from the load-indentation tests.

Sample No.	Water Ice Content (wt %)	Average Specific Penetration (kN/mm)	Predicted UCS (MPa)
5	0.01	1.2	1.8
12	0.01	0.8	1.3
TS2	0.25	0.7	1
TS1	0.32	2	3.4
3	1.48	9	13.8
4	1.30	5	7.8
10	1.03	5	7.7
11	0.57	4	5.6
1	8.80	20	31.2
2	8.56	28	43
8	8.38	24	36.4
9	7.88	27	41.7
6	10.97	46	70.7
7	10.17	47	71.5
57	11.80	61	92.2
58	11.60	62	94.8

The highest water ice concentration used in the load-indentation testing was ~12%. The strength of this material is high, with a SP of 62 kN/mm and a predicted UCS of ~95 MPa (Table 5). The direct UCS measurement of the sample with 12.7% water ice was similar at 102-104 MPa. This is in the range of relatively strong rock. Further, they failed in series of very small and brittle steps (Fig. 11-12). These features indicate that narrow spacing, possibly below 50 mm, would be more suitable.

In general, terrestrial cutter spacing selection tends to be conservative. Narrower spacings allow an excavator to fragment hard rock if encountered unexpectedly, even if not working as efficiently as wider spacings in relatively softer rocks. Even though this consumes additional energy, it allows an extra margin to deal with unexpectedly difficult lenses and hard inclusions. Such a contingency factor has been shown to be worthwhile through decades of mechanical excavation practice.

Cutter Penetration. Selection of the target penetration of the cutters into the material is a function of force required to achieve a known penetration (Fig. 7, 8-12). The higher the load capacity of the bit (and supporting subsystems of the machine) the deeper the penetration and, for a given S/P ratio, the wider the spacing. This leads to the largest chips and the most efficient cutting. Naturally, deeper cutter penetration can be achieved in weaker material for the same energy. In load-indentation tests, the weak material (water ice concentration below 1.5%) reached significant penetration before the indenter experienced any load. In harder materials (*e.g.* the 8-10% water ice range), much higher loads were recorded at similar ranges of penetration.

As the cutterhead rotates and moves forward through the ice-bearing material, only a small area of the cutterhead perimeter is in contact the regolith. For an appropriate cutting geometry and cutter placement, no more than two cutters will be cutting at any time. The penetration for each cutter changes as the cutter moves along the area or arc of contact, as shown in Fig. 21.

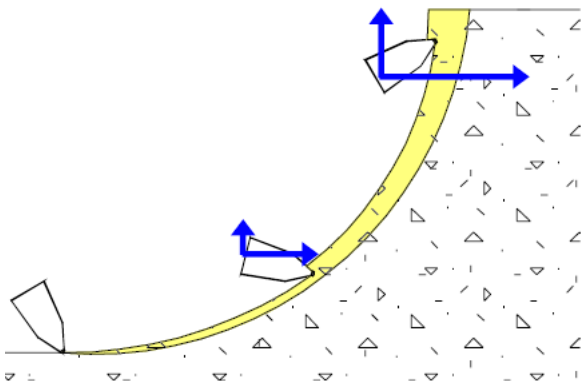

Fig. 21. Qualitative cutting force variation (blue) due to cutter penetration (yellow), which is due in turn to rotational position.

This constant change in penetration along with the change in cutter position means that the force on a cutter changes during its passage along the arc. The increasing penetration also increases the cutting forces. The computerized performance prediction model uses the actual 3D geometry of the cutterhead and the cutting area, including the true penetration, to estimate the forces, torque and power requirements of the excavator.

Excavation System

Following fragmentation of the *in situ* regolith or regolith-ice composite, the excavation system must then pick up the cut material and transport it to the next step of the process. This is best accomplished by a single machine. Transportation of the mined material to the base can be performed by shuttling lunar rovers.

Differences between Test and Lunar Conditions

The ice-regolith samples provide a good foundation of the potential mechanical properties that may be encountered. However, they were formed and tested under conditions quite different than the expected lunar conditions. Table 6 compares several characteristics between the ice-regolith samples tested in this study and the expected ice-regolith deposits in the permanently-shadowed regions near the lunar poles. A brief discussion of the potential effects of these differences follows.

The expected temperatures in the permanently-shadowed craters on the Moon (30-50 K) are lower than the temperature of the test samples (77 K). However, this difference in temperature is not expected to significantly affect the mechanical properties of the ice-regolith mixtures. The strength of the ice increases approximately 5 to 10 times with temperature decrease from 273 K to 150 K. The strength of the ice below 150 K remains approximately constant (Ivanov, 2001). Therefore, reducing the temperature from 77 K to 30 K is expected to have little or no effect on the mechanical properties of the ice-regolith mixture.

Table 6. Test conditions versus expected lunar polar conditions.

Trait	Test	Lunar
Temperature	~77 K	30-50 K
Pressure	~1 atm	hard vacuum
Anisotropy	isotropic	unknown
Ice Form	crystalline	unknown
Ice Content	0-11 wt%	1.5 ± 0.8%, local variation unknown
Compaction Method	static compression or vertical vibration	3-dimensional vibration
Relative Density	1.8-2.1 g/cm^3	1.3-2 g/cm^3
Simulant Mechanical Properties	JSC-1 lunar simulant	lunar polar soil

The samples were tested under ambient laboratory pressure. It is not known what effect, if any, that the presence of the air has on their behavior. To determine if this does have an effect, two identical test samples would be prepared, with one tested under vacuum conditions and the other one in ambient air. The effect on SP and SE of a sample tested at ambient temperature and pressure compared to one tested under vacuum conditions is expected to be quite small.

The particle size distribution of the soil and variations in the water content will affect the mechanics of its fragmentation and excavation. For example, a mixture of homogeneous particle sizes (soil and/or ice) behaves much differently than fine soil containing large ice lenses. A broad size distribution of lunar soil particles with thin ice coatings will behave differently than interspersed layers of ice and soil. The most likely configurations of lunar cold trap deposits are thought to be (Duke et al., 1998; Rice et al., 2000):

- Finely granular – formed by gardening of soil with introduction of ice grains.
- Ice chunks mixed with the regolith – formed by gardening of comet ice layers.
- Solid ice/regolith layers – formed by continuous accumulation of ice and diffusion of water.
- Trapped hydrogen gas from the solar wind – expected to behave similarly to dry regolith.

On Earth, ice acts as a cementing agent in unconsolidated materials, increasing their cohesion and thus increasing their resistance to cutter penetration. However, ice solidification within already well-consolidated material can decrease its strength by inducing local rupturing. The rapid increase in regolith density and cohesion observed within the first 60 cm of lunar regolith depth may cross the threshold between these two classes of behavior. It is unknown if ice particles in close proximity will bond together over long periods of time or if they will remain separate entities. Due to the uncertainties in the distribution of water ice within the lunar soil, homogenous mixtures of water and simulant were compacted and frozen for this study. These samples probably represent some of the strongest ice-regolith mixtures that will be encountered on the Moon.

The variation of the uniaxial compressive strength of frozen soils as a function of their water content is basically the same for all types of frozen soil. Strength of Frozen-Dry soil is at a certain level, which increases rapidly with increasing water content until the soil becomes saturated. As the water content of the soil increases beyond the saturation level, the strength of the mixture decreases below the compressive strength of pure ice.
The JSC-1 lunar simulant was designed to be chemically, mineralogically, and texturally similar to a mature lunar mare regolith (low titanium). The glass-rich character of JSC-1 (~50%) has quite different properties compared with other lunar simulants that were made entirely of comminuted crystalline rock, but with properties that are similar to lunar mare near surface regolith. While JSC-1 is a good lunar mare simulant, the properties of lunar highland regolith have some fundamental

differences (Carter *et al.*, 2004). The composition of the soil in the polar regions is not known, but it is believed to be closer to highlands regolith than to mare regolith. JSC-1 was the best chemical and mechanical lunar simulant available.

CONCLUSIONS AND RECOMMENDATIONS

The results of these experiments on lunar simulant JSC-1 to date have stimulated the following conclusions:

- Even at low water ice concentrations, compacted and frozen JSC-1 lunar regolith simulant behaves more like rock than like unconsolidated granular material.
- Frozen, compacted JSC-1 simulant becomes notably more difficult to excavate as its water ice content increases.
  - Higher specific penetration and specific energy requirements.
  - Higher unconfined compressive strength.
  - Smaller excavated volumes.
- If they exist, water ice deposits on the Moon will likely require mechanical excavators.
  - Simple buckets or scoop excavators will work well with dry and lightly compacted regolith on the lunar surface.
  - Robust conical bits mounted on a rotating cutterhead will be needed to recover subsurface lunar ice deposits.

A prototype cutterhead has subsequently been designed and built for lunar regolith excavation based on the results of load-indentation tests and UCS measurement of the compacted JSC-1 lunar regolith simulant at ~77 K, and full-scale linear cutting of a limestone that behaves similarly to frozen, partially saturated JSC-1. The prototype cutterhead is currently being tested in a variety of materials, ranging from the limestone to weak concrete mixtures that simulate the potential range in excavatability of the lunar regolith. Machine operating parameters as well as production rates have been estimated from the results of the testing completed to date, including full-scale linear cutting tests using actual conical bits. Rotary cutting tests are underway. More detailed study of the regolith and its response to mechanical excavation technology is needed to develop accurate and precise estimates of cutting rate and to evaluate the feasibility of using such systems for lunar mining and construction activities.

ACKNOWLEDGEMENTS

The work reported is being supported by the NASA Kennedy Space Center through Small Business Innovative Research (SBIR) Phase I and Phase II contracts, in addition to internal research and development funding by Orbital Technologies Corporation (ORBITEC).

Jim Mitchell's work on lunar regolith provided vital information for the planning and execution of this research. The late Richard Gertsch was the inspiration and a key contributor to much of the work reported here.

REFERENCES CITED

Boynton, W.V., W.C. Feldman, S.W. Squyres, T.H. Prettyman, J. Brückner, L.G. Evans, R.C. Reedy, R. Starr, J.R. Arnold, D.M. Drake, P.A.J. Englert, A.E. Metzger, Igor Mitrofanov, J.I. Trombka, C. d'Uston, H. Wänke, O. Gasnault, D.K. Hamara, D.M. Janes, R.L. Marcialis, S. Maurice, I. Mikheeva, G.J. Taylor, R. Tokar, and C. Shinohara [2002] "Distribution Of Hydrogen In the Near Surface Of Mars: Evidence For Subsurface Ice Deposits," *Science*, Vol 297, pp 81-85.

Brown, M.E. and Calvin, W.M. [2000] *Science*, Vol 287, p 107.

Carrier, W. D., S. W. Johnson, R. A. Werner and R. Schmidt. [1971] "Disturbance in samples recovered with the Apollo core tubes," Proc Second Lunar Science Conf, Geochimica et Cosmochimica Acta Supplement 2, 3:1959-1972. MIT Press.

Carrier, W. D., L. G. Bromwell, and R. T. Martin. [1972] "Strength and compressibility of returned lunar soil (abstract)," Lunar Science-III (ed. C. Watkins) pp 119-121, Lunar Science Institute Contract No. 88.

Carter, James L., McKay, David S., Taylor, Lawrence A., and Carrier, David [2004] "Lunar Simulants: JSC-1 is Gone; The Need for New Standardized Root Simulants," Space Resources Roundtable VI, Golden, CO.

Cherkasov, I. I., V. M. Vakhnin, A. L. Kemurjian, L. N. Mikhailov, V. V. Mikheyev, A. A. Musatov, M. I. Smorodinov, and V. V. Shvarey [1968] "Determination of the physical and mechanical properties of the lunar surface layer by means of Luna 13 automatic station," Moon and Planets II:70-76.

Christensen, E. M., S. A. Batterson, H. E. Benson, C. E. Chandler, R. H. Jones, F. R. Scott, E. N. Shipley, F. B. Sperling, and G. H. Sutton [1967] "Lunar surface mechanical properties-Surveyor," I. Jour Geophys Res, Vol 72, pp 801-813.

Christensen E. M., S. A. Batterson, H. E. Benson, R. Choate, R. E. Hutton, L. D. Jaffe, R. H. Jones, H. Y. Ko, F. N. Schmidt, R. F. Scott, R. L. Spencer, R. B. Sperling, and G. H. Sutton [1968a] "Lunar surface mechanical properties, in Surveyor VI, a preliminary report," NASA SP-166: 41-95.

Costes, N. C., W. D. Carrier, J. K. Mitchell, and R. F. Scott [1969] "Apollo 11 soil mechanics investigation," Apollo 11 Preliminary Science Report, NASA SP-214:85-122.

Costes, N. C., W. D. Carrier, J. K. Mitchell, and R. F. Scott [1970] "Apollo 11: Soil mechanics results," Journal of Soil Mechanics and Foundations Division, ASCE 96:2045-2080.

Costes, N. C. G. T. Cohron, and D. C. Moss [1971] "Cone penetration resistance test-An approach to evaluating the in-plane strength and packing characteristics of lunar soils," Proc

Second Lunar Science Conf, Geochimica et Cosmochimica Acta Supplement 2, 3:1973-1983.

Dollinger, G.L. [1978] "Lab tests provide low-cost method for predictiing raise boring costs," Eng. Min. J., Vol/Issue: 179:1, pp 86-89.

Dollinger, G.L., H.J. Handewith, C.D. Breeds [1998] "Use of the Punch Test for Estimating TBM Performance," Tunnelling and Underground Space Tech incorporating Trenchless Tech Research, Vol 13 (4) pp. 403-408.

Duke, M., R. Gustafson, E. Rice, M. Chiaverini, W. Knuth, C. St.Clair, W. Rothbauer, D. Gramer, G. McIntosh [1998] "Development of Preliminary Models, Processes, and Experimental Systems for Utilization of Lunar Polar Ice," OTC-G066-FR-98-1, Final Report to NASA Johnson Space Center, ORBITEC, Madison, WI, April.

Gertsch, R.E. [2000] Rock Toughness and Disc Cutting. Ph.D. dissertation, University of Missouri-Rolla, Rolla MO 65401.

Handewith, Howard [

Heiken, Grant, David Vaniman, and Bevan M. French (eds). [1991] Lunar Sourcebook- A User's Guide to the Moon. Cambridge: Cambridge University Press.

Houston, H. J., and L. I. Namiq [1971] "Penetration resistance of lunar soils," Journal of Terramechanics 8:59-69.

Houston, W. N., H. J. Hovland, J. K. Mitchell, and L. I. Namiq [1972] "Lunar soil porosity and its variation as estimated from footprints and bouldertracts (abstract)," In Lunar Science-III.

Hovland, H. J. and J. K. Mitchell [1971] "Mechanics of rolling sphere-soil slope interaction," Final Report, Volume II of IV, NASA Contract 8-21432, Space Sciences Laboratory, University of California, Berkeley.

Ivanov, B.A. [2001] "Martian Upper Crust Strength Estimates (abstract)," Institute for Dynamics of Geospheres, Russian Academy of Science, Leninsky Prospect., 38-1, Moscow, Russia.

Jaffe, L. D. [1967] "Surface structure and mechanical properties of the lunar maria," Jour Geophys Res, Vol 72, pp 1727-1731.

Leonovich, A. K., V. V. Gromon, A. V. Rybakov, V. K. Petrov, P. S. Pavlov, I. I. Cherkasov, and V. V. Shvarav [1971] "Studies of lunar ground mechanical properties with the self-propelled Lunokhod-1," Peredvizhnaya Laboratoriya na Luna-Lunokhod-1, Chap 8, pp 120-135.
Mitchell, J. K., L. G. Bromwell, W. D. Carrier, N. C. Costes, and R. F. Scott [1971] "Soil mechanics experiment," Apollo 14 Preliminary Science Report, NASA SP-272:87-108.

Mitchell, J. K., L. G. Bromwell, W. D. Carrier, N. C. Costes, W. N. Houston, and R. F. Scott [1972] "Soil mechanics experiment," Apollo 15 Preliminary Science Report, NASA SP-289:7-1—7-28.

Mitchell, J. K., W. D. Carrier, W. N. Houston, R. F. Scott, L. G. Bromwell, H. T. Durgunoglu, H. J. Hovland, D. D. Treadwell, and N. C. Costes [1972] "Soil Mechanics," Apollo 16 Preliminary Science Report, NASA SP-315:8-1—8- 29.

Mitchell, J. K., W. D. Carrier, N. C. Costes, W. N. Houston, R. F. Scott, and H. J. Hovland [1972] Apollo 17 Preliminary Science Report, NASA SP-330:8-1—8-22.

Mitchell, J. K., W. N. Houston, R. F. Scott, N. C. Costes, W. D. Carrier, and L. F. Bromwell [1972] "Mechanical properties of lunar soil: Density, porosity, cohesion, and angle of internal friction," Proc Third Lunar Conf, Geochimica et Cosmochimica Acta Supplement 3, 3:3235-3253.

Moore, H. J. [1970] "Estimates of the mechanical properties of lunar surface using tracks and secondary impact craters produced by blocks and boulders," Interagency Report: Astrogeology 22. USGS, US Dept of Interior.

National Gypsum [1995]) Continuous Surface Mining, internal report, 1707 #2 Highway, P.O. Box 57, Milford Station, Nova Scotia, Canada B0N 1YQ.

Nordmeyer, E.F. [1967] "Lunar surface mechanical properties derived from track left by nine meter boulder," MSC Internal Note No. 67-TH-1, NASA.

Nozette, S., Spudis, P.D., Robinson, M.S., Bussey, D.B.J., Lichtenberg, C., and Bonner, R., "Integration Of Lunar Polar Remote-Sensing Data Sets: Evidence For Ice At the Lunar South Pole," Paper 2000JE001417, Jour Geophys Res E: Planets, Vol 106, no.10, 2001, pp 23253-23266.

Rice, E.E., R.J. Gustafson, and R.R. Teeter [2000] "Development of Lunar Ice/Hydrogen Recovery System Architecture", Final Report OTC-G083-FR-2000-1, Orbital Technologies Corporation (ORBITECTM), Madison, WI, NASA/NIAC Research Grant 07600-021, 1 January.

Stack, B. [1982] Handbook of Mining and Tunneling Machinery, John Wiley & Sons, 742 pp.

Scott, R. F. [1968] "The density of lunar surface soil," Jour Geophys Res, Vol 73, pp 5469-5471.

Scott, R. F. and F. I. Roberson [1967] "Soil mechanics surface sampler: Lunar tests, results, and analyses," Surveyor III Mission Report, Part II: Scientific Data and Results. Tech Report 32-1177:69-110. Pasadena, California: JPL.

Scott, R. F., and R. I. Roberson [1968] "Surveyor III-Soil mechanics surface sampler: Luna surface tests, results, and analysis," Jour Geophys Res, Vol 73, pp 4045-4080.

Scott, R. F. and F. I. Roberson [1969] “Soil mechanics surface sampler,” Surveyor Program Results, NASA SP-184:171-179.

Scott, R. F., W. D. Carrier, N. C. Costes, and J. K. Mitchell [1970] “Mechanical properties of the lunar regolith,” Apollo 12 Preliminary Science Report, NASA SP-235:161-182.

Scott, R. F., W. D. Carrier, N. C. Costes, and J. K. Mitchell [1971] “Apollo 12 soil mechanics investigation,” Geotechnique 21:1-14.

Tsytovich, N. A. [1975] The Mechanics of Frozen Ground. New York: McGraw-Hill.

Vinogradov, A. P. [1971] Preliminary data on lunar ground brought to earth by automatic probe Luna 16,” Proc Second Lunar Science Conf, et Geochimica Cosmochimica Acta Supplement 2, 1:1-16.

Young, E. [2000] Science Vol 287, p 53.